ELSEVIER

Modeling the influence of anode–cathode spacing in a pulsed discharge nozzle

B.H.P. Broks [a], W.J.M. Brok [a], J. Remy [a], J.J.A.M. van der Mullen [a,*], A. Benidar [b], L. Biennier [b], F. Salama [c]

[a] Department of Applied Physics, Eindhoven University of Technology, P.O. Box, 513, 5600 MB, Eindhoven, The Netherlands
[b] Laboratoire de Physique des Atomes, Lasers, Molécules et Surfaces (PALMS), UMR CNRS 6627, Université de Rennes 1, 35042 Rennes Cedex, France
[c] NASA-Ames Research Center, Space Science Division, Moffett Field, CA 94035-1000, USA

Abstract

The pulsed discharge nozzle (PDN) is a spectrochemical source that is designed to produce and cool molecular ions in an astrophysically relevant environment in the laboratory with limited fragmentation. In order to gain a better understanding of the PDN and to optimize the yield of molecular ions and radicals in the PDN source, a parameter study of the influence of the interelectrode distance on the plasma properties is carried out by means of a discharge model, providing a qualitative as well as a quantitative picture of the plasma. We model the electron density and energy, as well as the argon ion and metastable atom number density for various interelectrode distances. The results reveal that increasing the interelectrode distance does not significantly influence the plasma at the cathode and at the anode. However, a positive column forms between the electrodes, which increases in length as the interelectrode distance increases. This is an additional evidence that the PDN is a glow discharge. This positive column does not contribute significantly to the formation of metastable argon atoms. Because metastable argon is thought to be the primary agent in the formation of molecular ions through Penning ionization of the neutral molecular precursor there is no benefit to be expected from an increase of the interelectrode distance. In fact, electron impact dissociation of the molecules in the column might even make the source less efficient for longer column lengths. The simulations presented here provide physical insight into the characteristics of interstellar species analogs in laboratory experiments.
© 2005 Elsevier B.V. All rights reserved.

1. Introduction

Interstellar dust is known to contain complex carbon molecules, such as polycyclic aromatic hydrocarbons (PAHs) [1]. Observational, laboratory and theoretical studies have shown that PAHs, in their neutral and ionized form, are an important component of the interstellar medium. PAHs might be responsible for two phenomena that have challenged the astrophysical community for over a century: the unidentified infrared bands observed in the emission spectrum of the interstellar media, and the diffuse interstellar bands seen in the visible and the near infrared absorption spectrum of diffuse interstellar clouds [2]. In order to assess the PAH proposal, which was first introduced by Leger and Puget [3] and by Allamandola et al. [4], we are constrained to compare astronomical observations with laboratory data, obtained under conditions that come close to those that reign in the interstellar medium. This places certain demands on the spectrochemical source used to ionize PAHs: the background gas must be at cryogenic temperature, and PAHs must be ionized in their ground state. Supersonic plasma sources meet these demands [5], because they produce metastables which are capable of soft Penning ionization of PAHs [6].

These sources operate by evaporating and seeding PAHs, which are large and nonvolatile molecules, in a noble carrier gas. The PAHs are cooled down and stabilized in the supersonic expansion. Recently, supersonic plasma sources have been used to generate cold PAH cations in the gas phase

* Corresponding author. Tel.: +31402474043; fax: +31402456050.
E-mail address: j.j.a.m.v.d.mullen@tue.nl (J.J.A.M. van der Mullen).

and combined to cavity ring down spectroscopy to measure their optical absorption spectra [7–9].

Such sources offer a powerful tool to produce and investigate radicals and ions, which are translationally and rotationally cold [10]. Supersonic expansion sources with long-slit orifices have been particularly proven to be efficient in generating high column densities of molecular ions and radicals, because of their geometry [11].

The pulsed discharge nozzle (PDN) source, which has been developed at NASA Ames [7], is such a supersonic source that can produce PAH metastables. The geometry of the PDN is schematically illustrated in Fig. 1. It is based on a slit mounted in a vacuum vessel. The gas shutter runs at 10 Hz and typically opens for a duration of 1.2 ms , generating intense short gas pulses with flow rates of 8 cm^3 per pulse. Two negatively biased jaws forming the cathode are mounted on each side of the 200 µm wide by 10 cm long slit and are 400 µm apart. They are insulated from the anode by a Macor© spacer plate which is 1.5 mm.

On the left hand side, neutral gas, in our case argon, enters with a pressure of approximately 10^5 Pa. The right hand side opening originates in a vacuum chamber, which is pumped to a backing pressure of 20 Pa. Because of this steep pressure gradient, the gas flows through the discharge region and expands supersonically in the vacuum chamber.

A negative voltage of several hundreds of volts (through 1 kΩ ballast resistors) is applied for 500 µs during the gas pulse. The plasma is thus generated in the expanding gas. The geometry of the source leads to a residence time of a few microseconds for the molecules in the active region of the discharge.

In order to interpret the results of the measurements on this source, and compare them to the measurements done on the astrophysical medium, it is desirable to understand the operation of the source so one knows in what form and what environment the species that is to be analyzed is produced. Furthermore, understanding a source facilitates optimizing it.

The plasma generated in the PDN source has been qualitatively analyzed in Refs. [12,13]. Estimates of the electron temperature and electron density in the plasma were obtained in these studies but do not provide a full and comprehensive description of the plasma properties by themselves.

In order to obtain a quantitative insight in the discharge properties, a detailed numerical study of the device was made in Ref. [6]. In this study, a precalculated flow field was used as an input for a glow discharge model. The results matched the available experimental results very well. An important conclusion was that the PDN acts as a source of cold metastables. These metastables, rather than the electrons, are the spectrochemical agents that ionize the PAHs, doing so via Penning ionization. Furthermore, it was concluded from the current–voltage characteristic that the PDN is a glow discharge in the abnormal regime.

In Ref. [6], we have speculated that changing the geometry could improve the yield of ionized PAH in the source. In particular, it was thought that by increasing the spacer plate width and hence the interelectrode distance, the residence time of PAHs in the plasma is increased, which should result in a higher yield of PAH ions. We investigate this proposal by a numerical study of three PDN assemblies with an interelectrode distance of 1.5, 4 and 10 mm, respectively. The study will be carried out using the model outlined in Ref. [6]. By comparing the results for the various interelectrode distances, conclusions can be drawn about the impact of the interelectrode distance on the source efficiency in the production of cold molecular ions. Furthermore, additional insight into the physics of the source may be gained and can lead to improvements of the source, such as a reduced dissociation of molecules.

Of equal importance is the additional physical insight in the plasma that produces the spectrochemical species. It was concluded in Refs. [12,13] that the plasma behaves as a glow discharge. This means that lengthening the device could lead to the formation of plasma regions, e.g. a positive column, that are not present in a shorter device [31,32].

We will start by giving a short outline of the modeling procedure. Particular emphasis is put on the geometry of the PDN source used in Refs. [7–9]. Then, a brief discussion of the general results will be given, where we compare several simulation results which are obtained when the interelectrode distance is set at 1.5 (PDN 1), 4 (PDN 2) and 10 mm (PDN 3) long, respectively. Conclusions will be drawn about the operation of the source.

2. The model

In this section, we will describe the model that is used to compute the plasma in the PDN. The fundamental assumption in the model is that the plasma does not influence the flow. This is justified by the low degree of ionization that is prevalent in the PDN. It allows us to treat the flow separately, and use the results as input for the plasma calculation. We use a two-dimensional model in which it is assumed that the slit is infinitely long in the z-direction. The length of the slit in the z-direction is indeed much longer than in the other dimensions, justifying this assumption.

2.1. The plasma model

The model used to describe the PDN plasma in this study is basically the same as in Ref. [6]. It has also previously been
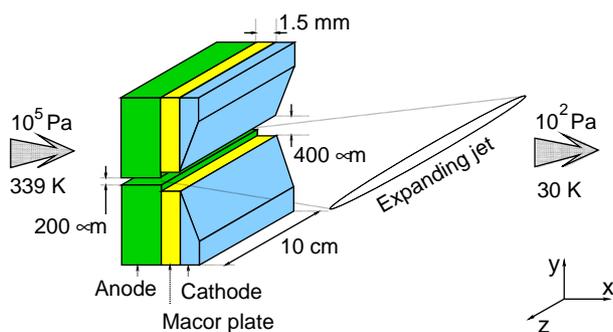

Fig. 1. (Color online) A schematic drawing of the pulsed discharge nozzle. The gas enters at atmospheric pressure on the left side and subsequently expands through the region between anode and cathode, where the discharge is generated. (Adapted from Ref. [6]).

used successfully to describe plasma display panel pixels [14], the ignition of compact fluorescent lamps [15] and the plasma needle [16] . A full description of the model can be found in Refs. [6,15] and references therein. We will give a very short overview of the basic model, and refer the reader to Refs. [6,15] for further details.

The plasma model is based on a two-dimensional time-dependent fluid approach. The conservation equations are solved in the drift-diffusion approach for six species, the electron, e, and four argon species, Ar^+, Ar^*, Ar^{**} and Ar^*_r. The electrons e and argon ions Ar^+ are treated as species. The four $4s$ levels of Ar are lumped in the Ar^* species, which is considered metastable, because the electron impact cross section for creating a metastable $4s$ level is significantly larger than the cross section for creating a resonant $4s$ level. The second excited state, denoted Ar^{**}, represents the $4p$ manifold and higher levels. In order to account for collisional quenching of the two metastable states to the two resonant states in the $4s$ manifold, a third excited species Ar^*_r is specified, which is destroyed by deexcitation to the ground level. The gas flow is incorporated in the conservation equations as a source term. The electric fields are obtained by solving the Poisson equation.

For the electron energy, a conservation equation that includes source terms for the energy gained in the electric field and lost in collisions is solved. The electron transport and reaction rate coefficients were obtained from an external Boltzmann solver [17], using input data from Refs. [15,18–25].

2.2. The flow model

The flow influences the plasma in two ways. First, the flow is a momentum source for the species. This momentum source enters the drift-diffusion equations. This effect is particularly important for the neutral species, as there are no electric forces to modify their speed. Second, the background gas density
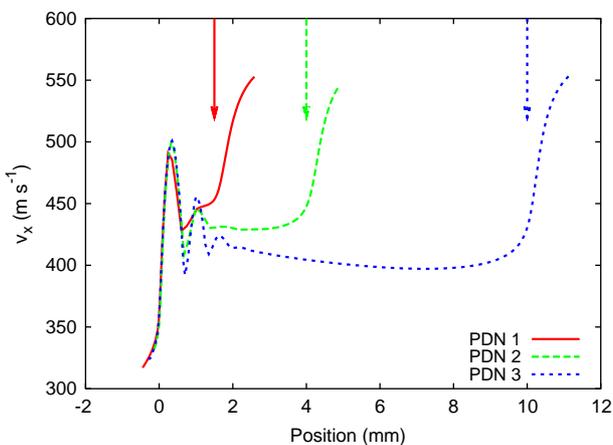

Fig. 3. (Color online) The Ar background density in the x-direction at the symmetry plane of the PDN, for a 1.5 mm interelectrode distance (PDN 1), a 4 mm interelectrode distance (PDN 2) and a 10 mm interelectrode distance (PDN 3). In all cases, the anode ends at $x=0$ mm. The position of the cathode is indicated by arrows (Adapted from Ref. [28]).

varies significantly in the device, affecting the reaction time and the diffusion of ionic species.

The PDN flow is modeled by a separate computer program MB-CNS that can calculate transient compressible flows in two-dimensional geometries. It is based on a finite volume formulation of the Navier–Stokes equations [26,27]. Details can be found in Ref. [28]. The bulk flow velocity in the x-direction at the symmetry plane of the PDN is plotted in Fig. 2. The Ar background density n_{Ar} in the x-direction at the symmetry plane of the PDN is plotted in Fig. 3. The PDN widens at two points: at the anode and at the cathode. At both points, the density drops and the velocity increases. In the interelectrode region, the flow remains supersonic.

There is a significant difference between the argon number density n_{Ar} near the cathode in PDN 1 and PDN 2 and 3, in particular off the symmetry plane.

Fig. 2. (Color online) The bulk flow velocity in the x-direction at the symmetry plane of the PDN, for a 1.5 mm interelectrode distance (PDN 1), a 4 mm interelectrode distance (PDN 2) and a 10 mm interelectrode distance (PDN 3). In all cases, the anode is positioned at $x=0$ mm. The position of the cathode is indicated by arrows (Adapted from Ref. [28]).
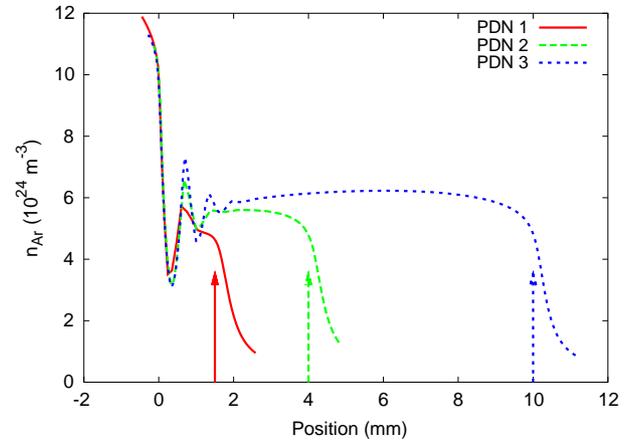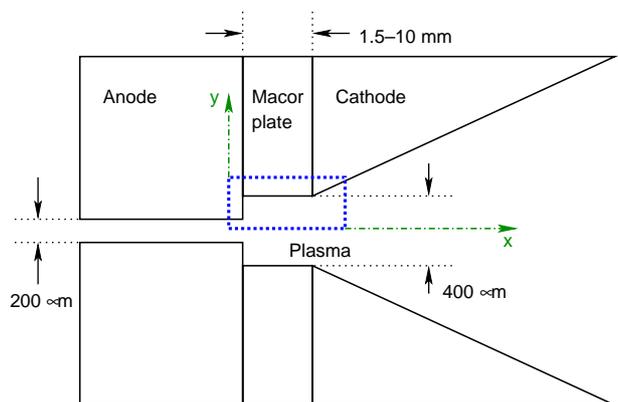

Fig. 4. (Color online) A schematic drawing of the geometry of the pulsed discharge nozzle. The size of the central plasma channel is exaggerated for clarity. The dashed rectangle is the part of the device that is simulated. The gas flows from a high-pressure source on the left to a vacuum chamber on the right. Note that we consider 3 situations, that differ from each other with respect to the length of the spacer plate. In PDN 1, this plate is 1.5 mm, in PDN 2, this plate is 4 mm, and in PDN 3, this plate is 10 mm (Adapted from [6]).

2.3. The geometry

The computation is carried out on a two-dimensional Cartesian grid. In our original study with an interelectrode distance of 1.5 mm [6] (PDN 1), a grid was used that consisted of 224 by 49 grid cells that were $12.5 \times 12.5 \ \mu m^2$. Increasing the interelectrode distance increases the length of the device in the x-direction, and therefore also the length of the grid needed. Increasing the grid length by simply adding grid cells would result in a model that is computationally too slow to be feasible (with the present code implementation). Hence, we increase the size of the cells in the x-direction. We use 200 by 50 grid cells with a $25 \times 12.5 \ \mu m^2$ cell size for PDN 2 (4 mm interelectrode distance), and 230 by 50 grid cells with a $50 \times 12.5 \ \mu m^2$ cell size for PDN 3 (10 mm interelectrode distance). The position of the grid in the device is schematically represented in Fig. 4.

3. Results and discussion

Using the model presented in Section 2, we simulated the pulsed discharge nozzle. By using the time-dependent equations described in Section 2 on a suitable starting condition, namely an argon plasma with an electron and ion density of $10^{11} \ m^{-3}$, a steady-state solution (differing less than 1% from the solution after a much longer time of 50 μs) is obtained in less than 15 μs . This is much shorter than the typical discharge time of 0.5 ms [7], meaning that stable conditions are present during most of the discharge. The discussion is restricted to this stable situation.

The plasma has a finite resistance. This means, that the voltage drop for a certain current in principle depends on the interelectrode distance. To be able to make a proper comparison between the various models, we will use a source voltage that results in the same average current density for all three cases, namely 1 mA mm^{-2}. At this current density, a current of 40 mA flows through the PDN.

3.1. General operation discussed using the results of PDN 1

The general operation of the discharge is treated in detail in Ref. [6]. We will summarize only the salient details here.
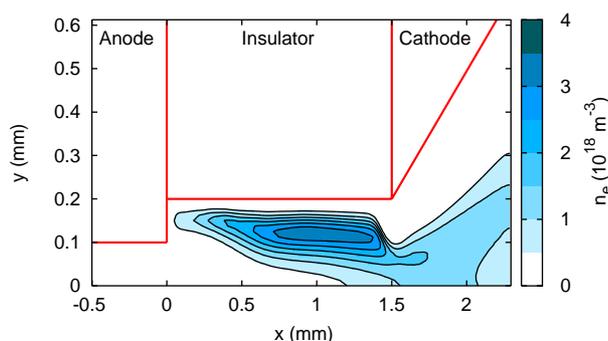

Fig. 5. (Color online) The steady-state electron density of PDN 1 for a source voltage of − 465 V. The color bar and isolines range from 0 to $4 \times 10^{18} \ m^{-3}$ in steps of $5 \times 10^{17} \ m^{-3}$. The bold lines indicate the different parts of the device.
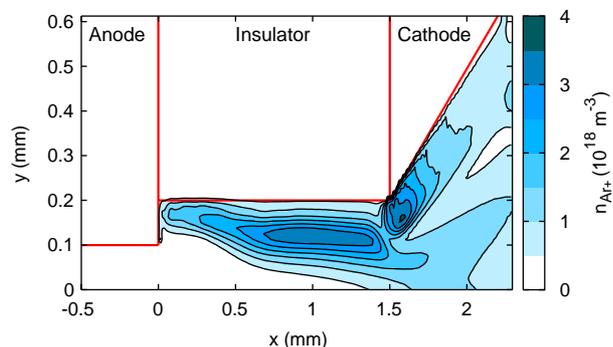

Fig. 6. (Color online) The steady-state Ar$^+$ density of PDN 1 for a source voltage of − 465 V. The color bar and isolines range from 0 to $4 \times 10^{18} \ m^{-3}$ in steps of $5 \times 10^{17} \ m^{-3}$. The bold lines indicate the different parts of the device.

The results discussed in Ref. [6] have been obtained for a source voltage of − 500 V. In order to have an average current density of 1 mA mm^{-2} , we will rather consider the results for − 465 V, which present no essential difference with the results at − 500 V.

The study of PDN 1, with a − 465 V source voltage, revealed that the discharge acts mainly as a source of Ar*, electrons e, and ions Ar$^+$. Both metastables and electron−ion pairs are mainly produced in two rather small areas of the discharge, namely near the anode and near the cathode tip, as shown in Figs. 5–7. There is a difference between the electron and Ar$^+$ distribution, especially near the cathode, where there is a cathode fall. The cathode fall is characterized by a peak in the n_{Ar+}, and a low n_e.

It is worth mentioning that the dominant formation mechanisms are different for both zones. Near the anode, where the average electron energy ε is about 7 eV, the dominant formation mechanism of Ar* is excitation of Ar to Ar*. Near the cathode, where the average electron energy is about 40 eV the dominant mechanism of Ar* is excitation of Ar to Ar** and subsequent decay to Ar*.

Comparing Figs. 5 and 7 shows that n_{Ar*} in the discharge is far larger than n_e . This observation, combined with typical reaction cross sections [29,30] for the processes under consideration and the typical electron energy calculated [6], leads to the conclusion that Ar* is the main agent in the formation of ionized PAHs.
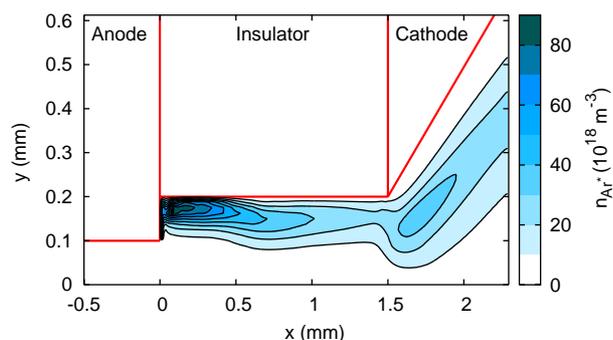

Fig. 7. (Color online) The steady-state Ar* density of PDN 1 for a source voltage of − 465 V . The color bar and isolines range from 0 to $90 \times 10^{18} \ m^{-3}$ in steps of $10 \times 10^{18} \ m^{-3}$. The bold lines indicate the different parts of the device.

The area immediately downstream from the cathode has a very low electron density, as is shown in Fig. 5. This is due to the presence of a cathode fall. The voltage drop over the cathode fall is large, accounting for the bulk of the voltage drop over the glow discharge plasma. The cathode fall is also clearly visible in Fig. 6 as an area with a high Ar^+ density. The Ar^+ density is highest near the tip of the cathode. This is because the background gas density is higher there than further upstream from the cathode.

3.2. Results and discussion for the PDN 2 configuration

A source voltage of -470 V is used in the model to obtain an average current density of 1 mA mm^{-2}.

Although one might expect that the voltage drop over the interelectrode distance would require PDN 2 to have a significantly higher source voltage than PDN 1 to produce the same average current density, this is not the case. The Ar density near the cathode is higher for PDN 2 than for PDN 1. Because higher Ar density causes the ionization rate at a given electron temperature and electron density to be higher, the cathode operation will be more efficient in this case. This means that the voltage drop over the cathode is lower for PDN 2 than for PDN 1, and this effect largely compensates the difference in interelectrode distance.

The electron density for PDN 2 is given in Fig. 8. The two active areas, one near the cathode and the other near the anode, are clearly visible, and are more distinct than for PDN 1. There is a clear dent in the electron density profile near the cathode. This is caused by the cathode fall, which is the most active near the tip of the cathode.

Comparing the n_e profile of PDN 2 in Fig. 8 with the n_e profile of PDN 1 in Fig. 5, we see that the n_e profiles in the anode region are similar.

Near the cathode, the situation is different. PDN 2 has a higher electron density near the cathode than PDN 1. This effect will be treated in more detail in the discussion of the PDN 3.

A clear difference between the n_e profiles of PDN 1 and PDN 2 is that the electron density peaks in the center of the discharge in most of the interelectrode distance of PDN 2

Fig. 9. (Color online) The steady-state Ar^+ density of the pulsed discharge nozzle with an interelectrode distance of 4 mm (PDN 2) for a source voltage of -470 V. The color bar and isolines range from 0 to 5×10^{18} m^{-3} in steps of 5×10^{17} m^{-3}. The bold lines indicate the different parts of the device.

while it peaks off the center in PDN 1. This is caused by the internal expansion of the plasma after the anode, which pushes the plasma to the wall. This process competes with the increased loss of electron–ion pairs by ambipolar diffusion near the walls. In PDN 1, the internal expansion covers a large part of the interelectrode space, while this part is much smaller in PDN 2. In this zone, the plasma density indeed peaks off the symmetry plane in both cases. In the interelectrode space of PDN 2 that lies after the expansion, the electron density indeed peaks at the symmetry plane.

The Ar^+ density for PDN 2 is given in Fig. 9. Comparing Figs. 8 and 9 shows that the plasma is close to quasineutral, except for the cathode fall. The cathode fall of PDN 2 is more strongly concentrated at the tip of the cathode than the cathode fall of PDN 1.

The Ar^* density for PDN 2 is given in Fig. 10. Ar^* is mainly produced near the anode and near the cathode and is subsequently transported downstream. While the density of Ar^* is highest near the anode, the production is in fact highest near the cathode. This is caused by the fact that the bulk velocity is low near the anode, while it is much higher near the cathode. Hence, the metastables generated near the
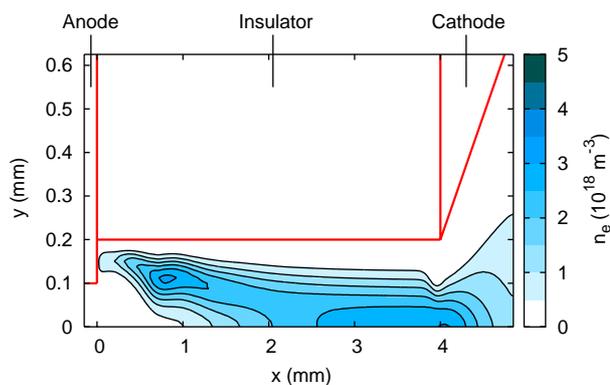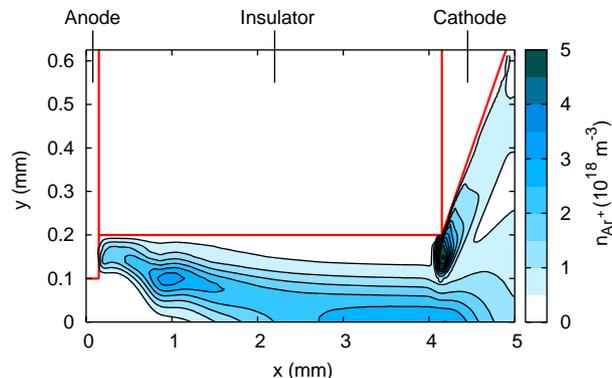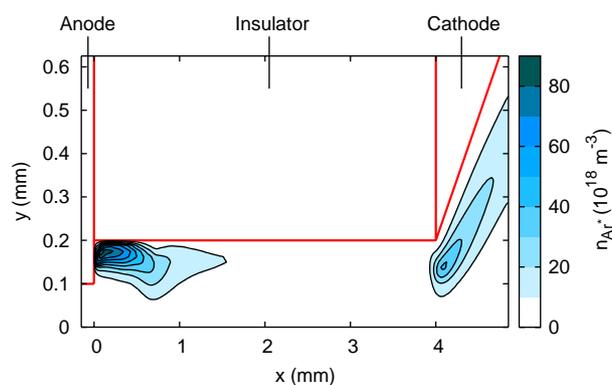

Fig. 8. (Color online) The steady-state electron density of the pulsed discharge nozzle with an interelectrode distance of 4 mm (PDN 2) for a source voltage of -470 V. The color bar and isolines range from 0 to 5×10^{18} m^{-3} in steps of 5×10^{17} m^{-3}. The bold lines indicate the different parts of the device.

Fig. 10. (Color online) The steady-state Ar^* density of the pulsed discharge nozzle with an interelectrode distance of 4 mm (PDN 2) for a source voltage of -470 V. The color bar and isolines range from 0 to 90×10^{18} m^{-3} in steps of 10×10^{18} m^{-3}. The bold lines indicate the different parts of the device.

cathode are carried away more effectively, resulting in a lower density there. For spectrochemical applications, the flux plays a more important role than the actual number density.

The plasma column produces less electron–ion pairs per Ar* produced than the production regions near the anode and cathode. Because the column is larger in a plasma with a larger interelectrode distance, fewer metastables are produced per electron–ion pair at the larger distances.

Comparing the n_{Ar*} profile of PDN 2 in Fig. 10 with the n_{Ar*} profile of PDN 1 in Fig. 7, we see that the anode regions are similar in the two cases. The bulk of the metastables generated near the anode decay before reaching the cathode in PDN 2, causing a clear distinction between the two production zones. The Ar* density is generally somewhat lower in PDN 2 than in PDN 1. The power dissipated in PDN 1 and PDN 2 is nearly equal. Because PDN 2 produces more electrons, mainly in the plasma column, it is not surprising that there is less power available for the production of Ar*, as observed. Furthermore, the average electron energy near the cathode is higher for PDN 1 (about 40 eV) than for PDN 2 (about 30 eV), because the cathode fall is larger.

The reaction rates predict that the ratio between produced metastables and electrons is higher at 40 than at 30 eV. This means that PDN 2 should produce less metastables per electron in the cathode region, as is observed.

3.3. Results and discussion for the PDN 3 configuration

A model of PDN 3 has been made. A source voltage of −610 V is now used in the model to obtain an average current density of 1 mA mm^{-2}.

The electron density for PDN 3 is given in Fig. 11. The plasma structure is quite similar to the plasma structure in PDN 2 shown in Fig. 8. There is an area with a high electron density at the anode, separated from the positive column. Again, the internal expansion of the gas pushes the plasma to the wall near the anode. The positive column fills the largest part of the discharge. A distinctive dent in the electron density profile near

Fig. 12. (Color online) The steady-state Ar$^+$ density of the pulsed discharge nozzle with an interelectrode distance of 10 mm (PDN 3) for a source voltage of −610 V. The color bar and isolines range from 0 to 4.5×10^{18} m^{-3} in steps of 5×10^{17} m^{-3}. The bold lines indicate the different parts of the device.

the cathode tip is visible, similar to the dent observed in PDN 1 (Fig. 5) and PDN 2 (Fig. 8). This dent is caused by the cathode fall.

The Ar$^+$ density for PDN 3 is given in Fig. 12. Comparing Figs. 11 and 12 shows that the plasma is close to quasineutral, except for the cathode fall. The cathode fall of PDN 3 is more strongly concentrated at the tip of the cathode than the cathode fall of PDN 1.

The Ar* density for PDN 3 is given in Fig. 13. The distribution of Ar* is quite similar to the distribution of Ar* in PDN 1 and PDN 2. There are two clearly separated zones with a high Ar* density, one near the anode and one near the cathode. In the positive column, n_{Ar*} is low and at both electrodes, n_{Ar*}, is lower in PDN 3 than in PDN 2.

3.4. General discussion

The spectrochemical characteristics of the source have been examined as a function of the interelectrode distance. We have investigated the trends induced by the variation in this parameter by considering the production of the two most important species for ion yield, namely n_e and n_{Ar+}, at a constant average current density of 1 mA mm^{-2}.
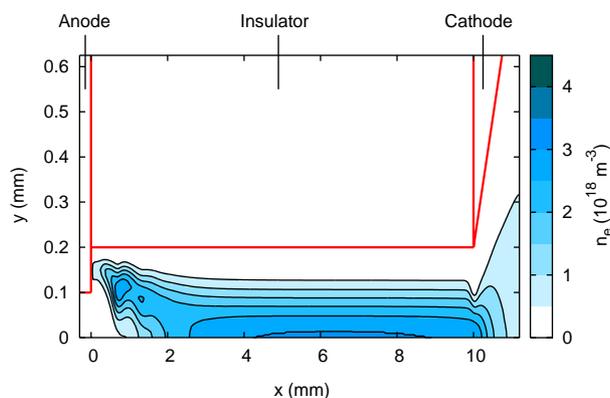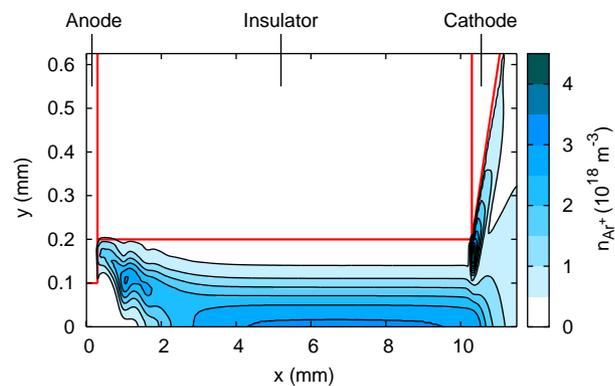

Fig. 11. (Color online) The steady-state electron density of the pulsed discharge nozzle with an interelectrode distance of 10 mm (PDN 3) for a source voltage of −610 V. The color bar and isolines range from 0 to 4.5×10^{18} m^{-3} in steps of 5×10^{17} m^{-3}. The bold lines indicate the different parts of the device.
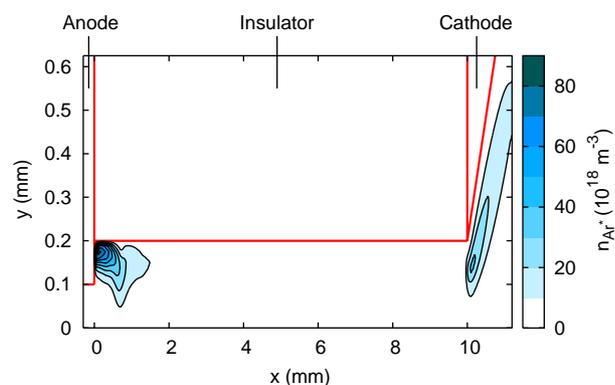

Fig. 13. (Color online) The steady-state Ar* density of the pulsed nozzle discharge with an interelectrode distance of 10 mm (PDN 3) for a source voltage of 610 V. The color bar and isolines range from 0 to 90×10^{18} m^{-3} in steps of 10×10^{18} m^{-3}. The bold lines indicate the different parts of the device.

The investigation of the electron and Ar* density shown in (Figs. 5, 6, 8, 9, 11 and 12) reveals that for longer interelectrode distances, a quasineutral positive column forms, which is not present in PDN 1. The electron and ion density near the anode do not vary significantly with varying interelectrode distance for the range of distances investigated in this work. This is consistent with the classical glow discharge theory [31,32]: when a glow discharge contains a positive column, the column length increases with the length of the discharge, while having little impact on the other features. This reinforces the idea suggested in Refs. [6,12,13] that the source operates as a glow discharge.

The presence of the positive column can also be shown in a different way. A positive column typically has a uniform electric field with a value that is small compared to the electric fields observed in the cathode and anode falls. The potential at $y = 193.75$ μm, which is close to the edge of the plasma at $y = 200$ μm, is given in Fig. 14 for the three different PDN configurations.

The voltage graphs in Fig. 14 all have two very distinct features: a cathode fall, visible as a sharp spike in the potential under the cathode tip, and an anode fall, which is visible as a rather steep voltage gradient near the anode. The spike is caused by the voltage drop over the cathode fall, which is necessary to extract electrons from the cathode. These features do not depend strongly on the length of the device, as is to be expected from classical glow discharge theory.

Between the cathode and the anode fall, an area with a lower and constant electric field of 3×10^4 V m^{-1} for PDN 2 and PDN 3 is visible. Because the background density is very similar for PDN 2 and PDN 3, it is expected that the field in the positive column is the same as well. In PDN 1, this area is very short, and the field strength is somewhat lower than for PDN 2 and PDN 3. This suggests that no real positive column is formed in PDN 1, a conclusion supported by the electron density map of Fig. 5 and experimental evidence [12]. A positive column field of 2.6×10^4 V m^{-1} is large. In this particular case, the small height of the plasma causes the
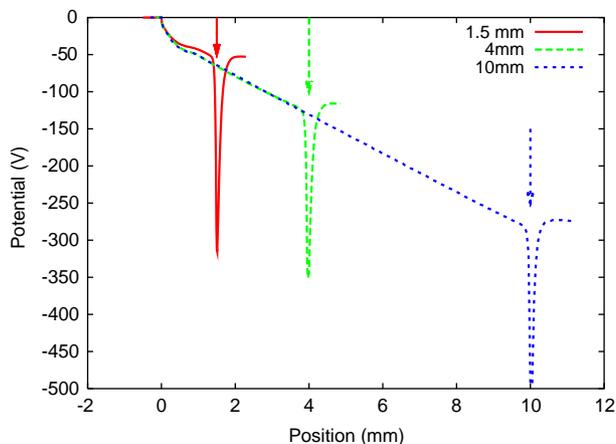
diffusive loss of metastables and electron–ion pairs to the wall to be very large [33,34]. The positive column field must therefore be large to compensate these losses in order to sustain the plasma.

Increasing the interelectrode distance apparently results in the formation and lengthening of a positive column. It is expected that a further increase of the electrode distance will result in a further lengthening of the positive column.

4. Conclusions

We have simulated the properties of the PDN for three different interelectrode distances, namely 1.5, 4 and 10 mm, with a source voltage that generates an average current density of 1 mA mm^{-2}.

The flow field changes significantly when going from the experimental PDN, which has an interelectrode distance of 1.5 mm, to PDN configurations with larger interelectrode distances. In the former case, there is however no clear distinction between the expansions at the anode and at the cathode, while in the latter cases, a clear distinction is observed. The Ar density near the cathode in PDN 1 is significantly lower than the Ar density near the cathode of PDN 2 and PDN 3, which causes the cathode fall of PDN 1 to be higher than the cathode fall of PDN 2 and PDN 3.

In the PDN with a 1.5 mm interelectrode distance, the production of the species that are the most relevant for ionization of the PAH, namely Ar* and e, is highest in two distinct zones: at the cathode and at the anode.

Increasing the interelectrode distance results in a larger separation of the two production zones. Furthermore, a positive column forms, stretching from under the cathode tip to about 1 mm from the anode. This positive column has a relatively high n_e, but a low n_{Ar*}. The formation of a positive column for longer device lengths reinforces earlier evidence that the source operates as a glow discharge.

Increasing the interelectrode distance length hence results in an increase of the area in which the PAHs are exposed to electrons. There is no increase however in the area in which the PAHs are exposed to Ar*. In fact, the Ar* density decreases slightly for increased interelectrode distance.

PAH molecules, which are the primary focus of spectrochemical research for the source under consideration have an ionization energy (~7 eV) [35] which is higher than the typical bond dissociation energy (~3–4 eV). Soft penning ionization by Ar* can produce PAH ions with limited fragmentation [6,7]. However, the average electron energy is so low (~4 eV) [6] in the positive column that far more electrons are capable of bond dissociation than of ionization. Hence, a high electron density is expected to be detrimental to the production of ionized PAHs.

A third possible reaction channel in the formation of PAH ions is by charge transfer reactions with Ar$^+$. This process, however, is likely to have a rather low reaction rate, because the thermal velocity of Ar$^+$ is low, about three orders of magnitude less than the electron thermal velocity. Furthermore, the density of Ar$^+$ is much lower than that of Ar*. Quantifying

Fig. 14. The potential at $y = 0.19375$ μm, which is just under the spacer plate, as can be seen in Fig. 4, for three different interelectrode distances. For all devices, the anode plate ends at $x = 0$. The anode region behaves identically in all three cases. In all cases, the potential is lowest under the tip of the cathode.

this contribution requires knowledge of the charge transfer cross section between the PAH and the Ar^+, which to the best of our knowledge is not known for singly ionized argon in low-energy collisions.

A quantitative analysis of the effect of varying n_{Ar*} and n_e on the formation of excited PAHs would require a simulation that specifically includes PAHs as species in the model. However, the lack of data for the PAH reactions makes this task difficult for the time being.

Acknowledgments

References

[1] F. Salama, Polycyclic aromatic hydrocarbons in the interstellar medium: a review, in: L. d'Hendecourt, C. Joblin, A. Jones (Eds.), Solid Interstellar Matter: The ISO Revolution, Les Houches Workshop, February 2–6 1998, EDP Sciences and Springer-Verlag, Les Ullis, 1999, pp. 65–+.

[2] A. Evans, The Dusty Universe, Ellis Horwood, London, 1994.

[3] A. Leger, J.L. Puget, Identification of the 'unidentified' IR emission features of interstellar dust? Astron. Astrophys. 137 (1984) L5–L8.

[4] L.J. Allamandola, A.G.G.M. Tielens, J.R. Barker, Polycyclic aromatic hydrocarbons and the unidentified infrared emission bands — auto exhaust along the Milky Way, Astrophys. J. 290 (1985) L25–L28.

[5] D. Romanini, L. Biennier, F. Salama, A. Kachanov, L.J. Allamandola, F. Stoeckel, Jet-discharge cavity ring-down spectroscopy of ionized polycyclic aromatic hydrocarbons: progress in testing the PAH hypothesis for the diffuse interstellar band problem, Chem. Phys. Lett. 303 (1999) 165–170.

[6] B.H.P. Broks, W.J.M. Brok, J. Remy, J.J.A.M. van der Mullen, A. Benidar, L. Biennier, F. Salama, Numerical investigation of the discharge characteristics of the pulsed discharge nozzle, Phys. Rev., E Stat. Phys. Plasmas Fluids Relat. Interdiscip. Topics 71 (2005) 063409.

[7] L. Biennier, F. Salama, L.J. Allamandola, J.J. Scherer, Pulsed discharge nozzle cavity ringdown spectroscopy of cold polycyclic aromatic hydrocarbon ions, J. Chem. Phys. 118 (2003) 7863–7872.

[8] O. Sukhorukov, A. Staicu, E. Diegel, G. Rouillé, T. Henning, F. Huisken, D2←D0 transition of the anthracene cation observed by cavity ring-down absorption spectroscopy in a supersonic jet, Chem. Phys. Lett. 386 (2004) 259–264.

[9] L. Biennier, F. Salama, M. Gupta, A. O'Keefe, Multiplex integrated cavity output spectroscopy of cold PAH cations, Chem. Phys. Lett. 387 (2004) 287–294.

[10] S. Davis, D.T. Anderson, G. Duxbury, D.J. Nesbitt, Jet-cooled molecular radicals in slit supersonic discharges: sub-doppler infrared studies of methyl radical, J. Chem. Phys. 107 (1997) 5661–5675.

[11] D.T. Anderson, S. Davis, T.-S. Zwier, D.J. Nesbitt, An intense slit discharge source of jet-cooled molecular ions and radicals, Chem. Phys. Lett. 258 (1996) 207–212.

[12] J. Remy, L. Biennier, F. Salama, Plasma structure in a pulsed discharge environment, Plasma Sources Sci. Technol. 12 (3) (2003) 295–301.

[13] J. Remy, L. Biennier, F. Salama, Plasma structure in a pulsed discharge environment, Plasma Sources Sci. Technol. 12 (4) (2003) 619.

[14] G.J.M. Hagelaar, M.H. Klein, R.J.M.M. Snijkers, G.M.W. Kroesen, Energy loss mechanisms in the microdischarges in plasma display panels, J. Appl. Phys. 89 (4) (2001) 2033–2039.

[15] W.J.M. Brok, J. van Dijk, M.D. Bowden, J.J.A.M. van der Mullen, G.M.W. Kroesen, A model study of propagation of the first ionisation wave during breakdown in a straight tube containing argon, J. Phys. D: Appl. Phys. 36 (16) (2003) 1967–1979.

[16] W.J.M. Brok, M.D. Bowden, J. van Dijk, J.J.A.M. van der Mullen, G.M.W. Kroesen, Numerical description of discharge characteristics of the plasma needle, J. Appl. Phys. 98 (1) (2005) 013302.

[17] BOLSIG, Boltzmann solver for the SIGLO-series 1.0, CPA Toulouse and Kinema Software, freeware, available at http://www.siglo-kinema.com/bolsig.htm (1996).

[18] A.V. Phelps, Z.L. Petrović, Review article: cold-cathode discharges and breakdown in argon: surface and gas phase production of secondary electrons, Plasma Sources Sci. Technol. 8 (1999) R21–R44.

[19] K. Tachibana, Excitation of the $1s_5$, $1s_4$, $1s_3$ and $1s_2$ levels of argon by low-energy electrons, Phys. Rev., A 34 (2) (1986) 1007–1015.

[20] P. Zapesochnyi, L.L. Shimon, Effective excitation cross sections of alkali-metal atoms colliding with slow electrons, Opt. Spectrosc. 11 (3) (1966) 155–157.

[21] R.H. McFarland, J.D. Kinney, Absolute cross sections of lithium and other alkali metal atoms for ionization by electrons, Phys. Rev. 137 (4A) (1965) A1058–A1061.

[22] L. Vriens, Calculation of absolute ionisation cross sections of He, He*, He^+, Ne, Ne*, Ne^+, Ar, Ar*, Hg and Hg*, Phys. Lett. 8 (4) (1964) 260–261.

[23] A.N. Klucharev, V. Vujnovic, Chemi-ionization in thermal-energy binary collisions of optically excited atoms, Phys. Rep. 185 (2) (1990) 55–81.

[24] N.L. Bassett, D.J. Economou, Effect of Cl_2 additions to an argon glow discharge, J. Appl. Phys. 75 (4) (1994) 1931–1939.

[25] S. Ashida, C. Lee, M.A. Lieberman, Spatially averaged (global) model of time modulated high density argon plasmas, J. Vac. Sci. Technol., A, Vac. Surf. Films 13 (5) (1995) 2498–2507.

[26] P.A. Jacobs, ICASE Interim Report 18, NASA Langley Research Center, 1991.

[27] P.A. Jacobs, MB-CNS: a computer program for the simulation of transient compressible flows, Department of Mechanical Engineering Research Report, The University of Queensland, 1996.

[28] L. Biennier, A. Benidar, F. Salama, Flow dynamics of a pulsed planar expansion, Submitted for publication Phys. Rev. E.

[29] S. Matt, B. Dünser, M. Lezius, H. Deutsch, K. Becker, A. Stamatoic, P. Scheier, T. Märk, Absolute partial and total cross-sections functions for the electron impact ionization of C_{60} and C_{70}, J. Chem. Phys. 105 (5) (1996) 1880–1896.

[30] J.M. Weber, K. Hansen, M.W. Ruf, H. Hotop, Penning ionization of C_{60} and C_{70}, Chem. Phys. 239 (1998) 271–286.

[31] M. Mitchner, m.C.H. Kruger, Partially Ionized Gases, John Wiley & Sons, 1973.

[32] Y.P. Raizer, Gas Discharge Physics, Springer, Berlin, 1991.

[33] B.H.P. Broks, Extending the capabilities of a plasma simulation model, Master's thesis, Eindhoven University of Technology, The Netherlands (2002).

[34] J. van der Mullen, G. Boidin, M. van de Sande, High-resolution electron density and temperature maps of a microwave plasma torch measured with a 2-D Thomsomscattering system, Spectrochim. Acta Part B 59 (2004) 929–940.

[35] K. Siegmann, H. Hepp, S. Frank, T. Malinowski, T.P. Martin, Multiphoton ionization mass spectroscopy of soot, PAH and fullerenes: the effect of photon energy, J. Aerosol Sci. 26 (1995) 661.